Biochimica et Biophysica Acta 1847 (2015) 1200–1211

Contents lists available at ScienceDirect

Biochimica et Biophysica Acta

journal homepage: www.elsevier.com/locate/bbabio

Physicochemical nature of interfaces controlling ferredoxin NADP$^+$ reductase activity through its interprotein interactions with ferredoxin

Misaki Kinoshita [a], Ju yaen Kim [a], Satoshi Kume [b], Yukiko Sakakibara [a], Toshihiko Sugiki [a], Chojiro Kojima [a], Genji Kurisu [a], Takahisa Ikegami [a,1], Toshiharu Hase [a], Yoko Kimata-Ariga [a,*], Young-Ho Lee [a,*]

[a] Institute for Protein Research, Osaka University, Yamadaoka 3-2, Suita, Osaka 565-0871, Japan
[b] Cellular Function Imaging Team, Division of Bio-function Dynamics Imaging, RIKEN Center for Life Science Technologies, Kobe, Hyogo 650-0047, Japan

ARTICLE INFO

Article history:
Received 13 April 2015
Received in revised form 27 May 2015
Accepted 29 May 2015
Available online 16 June 2015

Keywords:
Electrostatic interaction
Electron transfer
Enzyme activity
Binding thermodynamics
Driving force plot
Hydrophobic interaction

ABSTRACT

Although acidic residues of ferredoxin (Fd) are known to be essential for activities of various Fd-dependent enzymes, including ferredoxin NADP$^+$ reductase (FNR) and sulfite reductase (SiR), through electrostatic interactions with basic residues of partner enzymes, non-electrostatic contributions such as hydrophobic forces remain largely unknown. We herein demonstrated that intermolecular hydrophobic and charge–charge interactions between Fd and enzymes were both critical for enzymatic activity. Systematic site-directed mutagenesis, which altered physicochemical properties of residues on the interfaces of Fd for FNR /SiR, revealed various changes in activities of both enzymes. The replacement of serine 43 of Fd to a hydrophobic residue (S43W) and charged residue (S43D) increased and decreased FNR activity, respectively, while S43W showed significantly lower SiR activity without affecting SiR activity by S43D, suggesting that hydrophobic and electrostatic interprotein forces affected FNR activity. Enzyme kinetics revealed that changes in FNR activity by mutating Fd correlated with K_m, but not with k_{cat} or activation energy, indicating that interprotein interactions determined FNR activity. Calorimetry-based binding thermodynamics between Fd and FNR showed different binding modes of FNR to wild-type, S43W, or S43D, which were controlled by enthalpy and entropy, as shown by the driving force plot. Residue-based NMR spectroscopy of ^{15}N FNR with Fds also revealed distinct binding modes of each complex based on different directions of NMR peak shifts with similar overall chemical shift differences. We proposed that subtle adjustments in both hydrophobic and electrostatic forces were critical for enzymatic activity, and these results may be applicable to protein-based electron transfer systems.

1. Introduction

A large number of biological processes are regulated by intermolecular interactions among various biomolecules, small compounds, and metal ions under the control of kinetics and thermodynamics, with the aim of maintaining homeostasis [1–3]. The regulation of protein interactions with target molecules is of particular importance because misguided intermolecular interactions often lead to impaired enzymatic activities and protein functions, thereby resulting in dysfunctional organelles and numerous diseases [4].

One of the most controlled protein-based physiological processes is the electron transport chain in photosynthesis and respiration [5]. In these metabolic processes, a series of soluble proteins/enzymes and membrane protein complexes play pivotal roles in electron transfer by communicating with target and binding molecules in response to changes in environmental conditions such as variations in pH, temperature, and the redox state [6–8].

Detailed studies on enzyme activities and electron transfer rates based on the static and dynamic structures determined by X-ray crystallography and solution NMR spectroscopy have increased our understanding of the molecular mechanisms underlying electron flow and enzymatic activities in photosynthesis and respiration [3, 9–12]. Solution NMR spectroscopy and calorimetry have provided further information on the dynamic structures of proteins and molecular origins of intermolecular interactions for protein functions [3,13].

Several key electron-carrying proteins, such as plastocyanin and ferredoxin (Fd), have been identified in the chloroplasts of higher plants

Abbreviations: Fd, ferredoxin; PETF, plant-type photosynthetic electron transport ferredoxin; FNR, ferredoxin NADP$^+$ reductase; SiR, sulfite reductase; CD, circular dichroism; CSP ($\Delta\delta_{tot}$), chemical shift perturbation; FAD, flavin adenine dinucleotide; HSQC, heteronuclear single quantum correlation; ITC, isothermal titration calorimetry; NADPH, nicotinamide adenine dinucleotide phosphate; NMR, nuclear magnetic resonance; ΔH, enthalpy change; ΔS, entropy change; ΔG, Gibbs free energy; ΔC_p, heat capacity change.

* Corresponding authors.
E-mail addresses: a-yoko@protein.osaka-u.ac.jp (Y. Kimata-Ariga), mr0505@protein.osaka-u.ac.jp (Y.-H. Lee).
[1] Current address: Structural Epigenetics Laboratory, Graduate School of Medical Life Science, Yokohama City University, 1-7-29 Suehiro-cho, Tsurumi-ku, Yokohama 230-0045, Japan.

http://dx.doi.org/10.1016/j.bbabio.2015.05.023
0005-2728/

for photosynthesis [14,15]. Electron carrier proteins transport an electron to their physiological redox partner molecules in a manner that has been shown to depend on differences in redox potential [16]. On the other hand, well-regulated protein–protein interactions between electron-carrier proteins and redox partner proteins/enzymes were found to maximize efficient intermolecular electron transfer and relayed enzymatic reactions [8], which emphasized the consequences of the formation of electron transport-competent protein complexes. However, the dominant factors controlling interprotein interactions have not yet been examined in detail from the viewpoints of enzymatic kinetics and binding thermodynamics together with the determination of an available complex structure.

Fd is considered to be a good model protein because it transfers an electron obtained from photosystem I to several target enzymes, including ferredoxin-$NADP^+$ reductase (FNR), sulfite reductase (SiR), nitrite reductase (NiR), and hydrogenase [17], through the formation of electron transfer protein complexes [9,11,18]. Fd is a small acidic protein (~10.5 kDa) that accommodates the redox center of the [2Fe–2S] cluster [5]. Previous studies suggested that the negatively-charged residues of Fd stabilized a complex through complementary electrostatic interactions with the positively-charged residues of partner enzymes, as previously reported in Fd and FNR binding in photosynthesis and Fd and SiR binding in sulfur assimilation [11,18,19].

Although diverse biochemical methods are useful for indirectly elucidating the interprotein electrostatic interactions of Fd with several enzymes [20,21], the three-dimensional structure of the complex provides straightforward information for identifying interprotein interactions at the atomic level [22]. The complex structure between maize leaf Fd and FNR, which was the only available structure among several complexes between Fd and partner enzymes in plants, showed that interfaces mostly consisted of electrostatic interactions, including five salt bridges, a large number of hydrogen bonds, and hydrophobic contacts [22,23]. FNR is a relatively large multidomain enzyme (~35.5 kDa) that reduces $NADP^+$ to NADPH by transferring two electrons via flavin adenine dinucleotide (FAD) in FNR and hydride [23–25]. Solution NMR-based investigations on Fd further supported electrostatic interactions between the oppositely-charged residues of Fd and FNR [20,22,26].

A recent thermodynamic study using solution NMR spectroscopy and calorimetry reported that increases in the FNR backbone flexibility of regions remote from interfaces and dehydration from both apolar and polar surfaces were important for the formation of the Fd:FNR complex [3,22]. These findings indicated the contribution of hydrophobic interactions, which have received less attention than electrostatic contributions, to FNR activity. The strong potential for charge clusters on the surfaces of electron transfer proteins [25,27] and NMR invisible hydrophobic regions of Fd due to paramagnetic relaxation enhancements from the unpaired electrons of iron [9] may have led to the biased interpretation of electrostatic interactions by masking hydrophobic contributions.

By using the biochemical approaches of systematic site-directed mutagenesis and activity measurements in combination with the biophysical methods of isothermal titration calorimetry, solution NMR spectroscopy, and docking simulations, we herein investigated the contribution of hydrophobic interactions between Fd and FNR to FNR activity together with charge–charge interactions. We showed that the hydrophobic forces of Fd were also key to FNR activity together with conventional electrostatic forces, and that the delicate balance between these two forces regulated FNR activity by controlling interprotein interactions between Fd and FNR.

2. Materials and methods

2.1. Preparation of proteins

All site-directed Fd mutants on the hydrophobic surfaces of maize leaf-type Fd (Fd I) were prepared using a QuikChange Lightning Site-Directed mutagenesis kit (Agilent Technologies, USA) and recombinant maize-FdI plasmid DNA as a template [28]. The mutation sites and sequence integrity of the entire coding region were confirmed by DNA sequencing. Wild-type and mutant Fds were expressed from *Escherichia coli* BL21 (DE3) cells and purified according to previously described methods [29].

The preparation of recombinant maize leaf FNR (L-FNR I) and ^{15}N-labeled FNR was based on previous studies [19,30]. Fd and FNR concentrations were determined using the molar extinction coefficients of 9680 M^{-1} cm^{-1} at 423 nm and 10,000 M^{-1} cm^{-1} at 460 nm, respectively.

2.2. Assay for electron transfer activity of FNR

The nicotinamide adenine dinucleotide phosphate (NADPH)-dependent reduction of Fd by FNR was measured at 298 K, as described previously [19], by monitoring increases in reduced cytochrome *c* (Nacalai Tesque, Japan) at 550 nm in an assay mixture of 50 mM Tris–HCl buffer (pH 7.5) containing 50 μM NADPH, 20 nM FNR, 2.5 μM (Fig. 1C) or 1.25 μM Fd (Fig. 1E), and 200 μM cytochrome *c*, which represented the NADPH-generating system. The Michaelis constant (K_m) at 298 K and turnover number (k_{cat}) at various temperatures (288, 293, 298, and 303 K) were calculated by fitting to the following Michaelis–Menten equation:

$$v = \frac{k_{cat}[FNR]_0[Fd]}{[Fd] + K_m} \quad (1)$$

where *v* indicates the initial velocity of the catalytic reaction of FNR, and $[FNR]_0$ and [Fd] indicate the concentrations of FNR and Fd in the reaction mixture, respectively.

2.3. Assay for electron transfer activity of SiR

Fd-dependent sulfite reduction by SiR was assayed by monitoring the final product of cysteine using a reconstituted electron transfer system [11]. Reaction mixtures in 50 mM Tris–HCl (pH 7.5) consisted of 200 nM SiR, 2 mM $Na_2SO_3^{2-}$, 0.4 units of cysteine synthase, O-acetyl serine, and 10 μM (Fig. 1D) or 20 μM Fd (Fig. 1F). SiR reduction was initiated by an intermolecular electron transfer from Fd, which was reduced by $Na_2S_2O_4$. Reduced SiR sequentially converted sulfite to sulfide. Cysteine synthase, in the presence of O-acetyl serine, produced cysteine from sulfide. The reaction was stopped 0, 3, 6, and 9 min after reducing SiR by the addition of trichloroacetic acid at a final concentration of 20% (v/v). The solution was promptly centrifuged at 15,000 rpm for 3 min and 150 μl of the supernatant was collected. After the addition of 150 μl acetic acid and 150 μl acid-ninhydrin reagent to the supernatant, the solution was heated at 95 °C for 10 min. The addition of 450 μl ethanol to the solution allowed the production of cysteine to be monitored by increases in absorption intensity at 546 nm. Specific activity was obtained by the slope of time-dependent activity at each incubation time.

2.4. Circular dichroism (CD) measurements

All CD measurements of Fd solutions were performed in 50 mM Tris–HCl buffer (pH 7.5) using a J720 spectropolarimeter (Jasco, Japan) at 25 °C. Far-UV CD spectra at 0.2 mg ml^{-1} Fd (~20 μM) were recorded using a quartz cuvette with a 1-mm path length. Near-UV and visible CD spectra with 1 mg ml^{-1} Fd (~100 μM) were obtained using a quartz cuvette with a 1-cm path length. Spectra were expressed as mean residue ellipticity, [θ] (deg cm^2 $dmol^{-1}$), after subtracting the solvent background.

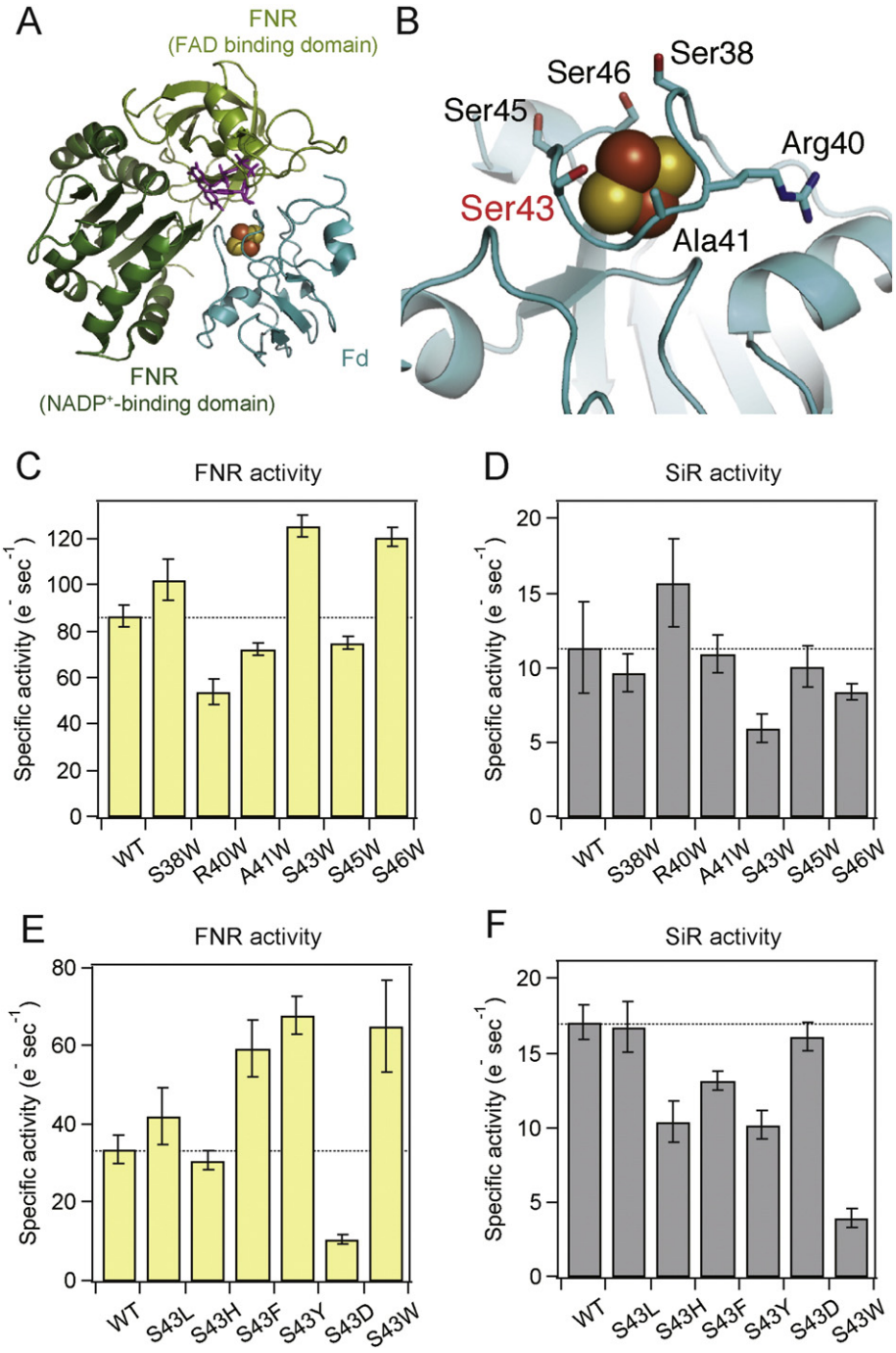

Fig. 1. Structure-based mutagenesis of Fd and enzymatic activity. (A–B) The structure of the Fd:FNR complex (PDB /1GAQ) (A) and position of Fd residues for mutations (B) are shown. FNR and Fd are displayed in green and light blue colors, respectively. FAD- and $NADP^+$-binding domains are shown in light and dark green, respectively. Red and yellow spheres in Fd represent iron and sulfur, respectively. Magenta sticks in FNR indicate FAD. (C–F) The results of the activity assay for FNR (C, E) and SiR (D, F) are shown with bar graphs.

2.5. Isothermal titration calorimetry (ITC) measurements

Protein solutions were dialyzed against 50 mM Tris–HCl (pH 7.5) and degassed for 3 min before being loaded into the calorimeter. Calorimetric experiments were performed with a VP-ITC instrument (GE-Healthcare Biosciences, USA) at 288, 293, 298, and 303 K. In the injection syringe, 1 mM FNR was titrated into 50 μM wild-type or mutant Fds in the ITC cell. Titration experiments consisted of 40 injections spaced at intervals of 400–500 s. The injection volume was 7 μl and the cell was continuously stirred at 264 rpm [3].

Observed enthalpy changes (ΔH_{bind}) for binding and the dissociation constant (K_d) were directly calculated from the integrated heat using the one-set of independent binding sites model supplied by the MicroCal Origin 7.0 software. The equation of this binding model was:

$$Q = \frac{n[P]_t \Delta H_{bind} V_0}{2}\left[1 + \frac{L_R}{n} + \frac{K_d}{n[P]_t} - \sqrt{\left(1 + \frac{L_R}{n} + \frac{K_d}{n[P]_t}\right)^2 - \frac{4L_R}{n}}\right] \quad (2)$$

where Q is the change in heat in the system, V_0 is the effective volume of the calorimeter cell (1.43 ml), L_R is the ratio of the total Fd concentration to total FNR concentration ($[P]_t$) at any given point during the titration, and n is the binding stoichiometry of Fd per FNR. Using ΔH_{bind} and K_d, the observed Gibbs energy change for binding (ΔG_{bind}) and observed

entropy change for binding (ΔS_{bind}) were obtained by thermodynamic relationships (Eqs. (3) and (4)) as follows;

$$\Delta G_{bind} = RT \ln K_d \quad (3)$$

$$\Delta G_{bind} = \Delta H_{bind} - T\Delta S_{bind} \quad (4)$$

where R is the gas constant and T is the temperature in Kelvins.

2.6. Solution NMR measurements of FNR

FNR samples uniformly labeled with ^{15}N were prepared using 50 mM Tris–HCl buffer (pH 7.5) containing 10% D_2O for ^{1}H–^{15}N heteronuclear single quantum correlation (HSQC) measurements. All HSQC spectra of 0.2 mM ^{15}N-labeled FNR in the absence and presence of 0.4 mM wild-type or mutant Fd (S43W and S43D) were obtained at 25 °C in an AVANCE-III H/D 800 spectrometer equipped with a cryogenic probe (Bruker BioSpin, Germany). Data were processed by NMRPipe and analyzed by Sparky [31].

A chemical shift perturbation ($\Delta\delta_{tot}$) in the cross-peaks of FNR by the addition of Fd was calculated using the relationship:

$$\Delta\delta_{tot} = \left[(\Delta\delta_H)^2 + (\Delta\delta_N \times 0.158)^2\right]^{0.5} \quad (5)$$

where $\Delta\delta_H$ and $\Delta\delta_N$ are the changes in the ^{1}H and ^{15}N chemical shifts in ppm, respectively. The weighting factor of 0.158 was used to adjust the relative magnitudes of the amide nitrogen chemical shift range and amide proton chemical shift range.

2.7. Computational docking simulation between FNR and Fd

Homology modeling of S43W- (S43W) and S43D-substituted Fd (S43D) was performed using the Modeller program v9.11 and crystal structure of wild-type Fd (PDB/3B2F) [12] for a template structure. The qualities of the modeled structures of the Fd mutants were confirmed using the VERIFY3D program [32].

The docking simulation between Fd (wild-type, S43W, or S43D) and FNR was performed using the HADDOCK easy interface server with semi-flexible refinements. Active residues for interaction restraints were defined based on the chemical shift perturbation data observed in our present and previous NMR studies [33] and were filtered for the accessible surface area calculated by VARDAR (version 1.8) [34]. The active residues of Fd and FNR obtained are listed in Table S1. Passive residues were defined automatically around the active residues. A total of 40 possible Fd:FNR complexes were obtained (see the Supplementary data section).

3. Results

3.1. Interface mutations differentially affected enzymatic activity between FNR and SiR

In order to examine the contribution of hydrophobic forces around serine 38 to 46 on the interface of Fd for FNR and SiR to enzymatic activities, we constructed six Fd mutants in which hydrophobicity was increased (S38W, R40W, A41W, S43W, S45W, and S46W) on the basis of our previous FNR-bound Fd structure (Fig. 1A and B), and performed FNR and SiR activity assays (Fig. 1C and D).

The mutants exhibited various activity changes. The SiR and FNR activities of R40W and S43W mutants were opposite (here designated as a partner enzyme-dependent activity change): R40W and S43W mutants exhibited an increase and decrease in SiR activity (Fig. 1D) and a decrease and increase in FNR activity (Fig. 1C), respectively. No recognizable activity changes were observed among the other mutants; however, the FNR activity of the S46W mutant increased (Fig. 1C).

Based on the largest change in activities depending on enzymes, high conservation in higher plants (Fig. S1), and locational importance for electron transfer between the [2Fe–2S] cluster in Fd and FAD in FNR, we focused on mutagenic analyses of serine 43. In order to obtain a more general insight into the effects of physicochemical properties on enzymatic activity, more Fd mutants were prepared in terms of hydrophobic and electrostatic natures: S43L, S43H, S43F, S43Y, and S43D.

The hydrophobic mutants, S43F, S43Y, and S43W, exhibited marked increases in FNR activities, whereas that of the S43D mutant was markedly decreased by increases in acidity, and the remaining mutants did not show significant activity changes (Fig. 1E). The SiR activities of the S43H, S43F, and S43Y mutants decreased and that of S43W was markedly reduced. However, no significant activity changes were observed with the S43L and S43D mutants (Fig. 1F).

3.2. NADPH-dependent FNR activity using wild-type and mutant Fds

We measured the steady-state kinetics of reductions in cytochrome *c* in order to determine the effects of site-directed mutations in Fd on FNR activity. We selected the two mutants, S43W and S43D because their enzyme activities markedly differed in a partner enzyme-dependent manner, i.e., a partner enzyme-dependent activity change (Fig. 1E and F). The maximum velocity (v) for reductions in cytochrome *c* at various concentrations of wild-type Fd was saturated at a low Fd concentration (less than 5 μM) at 298 K (Fig. 2A), indicating steady-state kinetics with the formation of the Fd:FNR complex. Thus, data were fit using the Michaelis–Menten equation (see the Materials and Methods section). The Michaelis constant (K_m) and turnover number (k_{cat}) were 2.1 μM and 53.5 s^{-1}, respectively (Table 1). The results obtained for the two variants also showed Michaelis–Menten kinetics. Although no significant changes were observed in k_{cat}, K_m values increased to 0.8 μM for S43W and 9.0 μM for S43D (Table 1).

The temperature dependence of k_{cat} was then examined. The k_{cat} values with wild-type Fd increased from 37.8 to 72.5 s^{-1} with elevations in temperature from 288 to 303 K (Fig. 2B and Table 1). The k_{cat} values with Fd variants showed a very similar temperature dependence to wild-type Fd. Accordingly, activation energy (E_a), which was deduced from the Arrhenius equation, was similar regardless of the types of Fds (Fig. 2C and Table 1). On the other hand, although the K_m values for wild-type and S43W Fds did not show a notable dependency on temperature, that for S43D varied in an opposite manner to the temperature increase (Fig. 2D and Table 1).

3.3. Investigation of structural changes in Fd mutants by various spectroscopies

We demonstrated whether structural changes were caused by substitution mutations using CD and absorption spectroscopy. In CD spectroscopy, we performed measurements at three regions of wavelengths: far-UV (195–250 nm) to examine the secondary structure (Fig. S2A), near-UV (250–300 nm) for the structure near aromatic residues (Fig. S2B), and visible (300–600 nm) regions for [2Fe–2S] for environment-containing clusters (Fig. S2C).

No significant changes were observed in the far-UV CD spectra of the three types of Fds (wild-type, S43W, and S43D), which indicated that the content of alpha helices, beta strands, and random coils was constant in all Fd variants. In the near-UV region, no significant differences were noted in the CD spectra among Fds. Only slight changes were observed in the visible-spectra near 500, 375, and 325 nm. This result indicated that appreciable geometry changes did not occur around the [2Fe–2S] clusters, which was further supported by absorbance spectra. Each of the absorbance spectra of the Fd variants was similar, except for the region near 280 nm of S43W (Fig. S2D), and was mainly attributed to the substitution of tryptophan, showing absorption near 280 nm.

We defined the mutation effects on Fd structures negligible for activities between FNR and each Fd variant. However, we did not exclude the

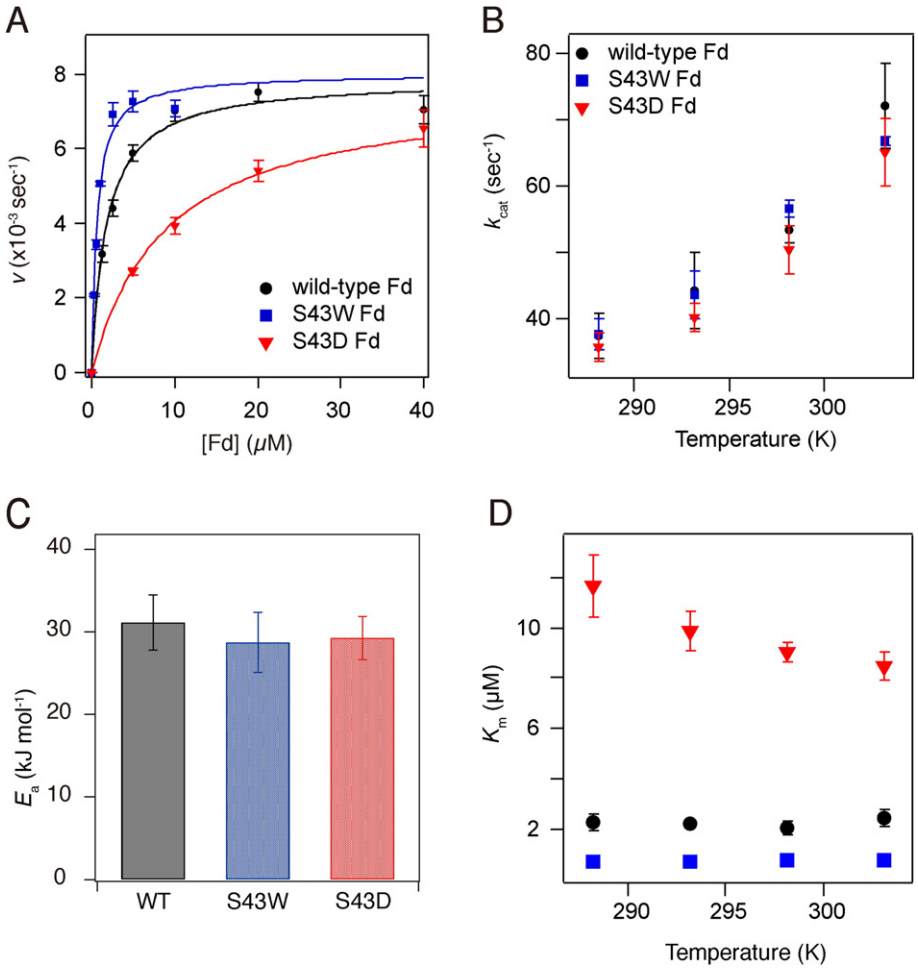

Fig. 2. FNR activity depended on mutations and temperature. (A) The steady-state kinetics of FNR based on the reduction of cytochrome *c* at 298 K are shown. The concentrations of wild-type Fd used were 1.25, 2.5, 5, 10, 20, and 40 μM while those of S43W Fd were 0.25, 0.5, 1, 2.5, 5, and 10 μM. S43D Fd was used at concentrations of 5, 10, 20, and 40 μM. The continuous lines indicate the fitting curves based on the Michaelis–Menten equation. (B) k_{cat} values were plotted against temperature. (C) Schematic bar presentations of activation energies (E_a). (D) Temperature dependence of K_m values. Values corresponding to wide-type, S43W, and S43D Fds are shown in black, blue, and red, respectively.

possibility that mutations may have caused changes in midpoint potentials in free Fd and/or FNR-bound Fd that may, in turn, have affected activities. A previous study reported that a mutation in S47A in Anabaena Fd, which corresponded to S45 in maize Fd, markedly affected the midpoint redox potential and rate of FNR reduction [35].

3.4. Thermodynamic characterization of Fd:FNR interactions monitored by calorimetry

We performed ITC measurements using three types of Fds (wild-type, S43W, and S43D) and FNR (Fig. 3) in order to examine thermodynamically interprotein interactions between Fd and FNR at the molecular level in solution.

The titration of wild-type Fd to FNR at 298 K showed a series of positive heat peaks, which indicated complex formation with heat uptake (Fig. 3A) and was consistent with our previous findings [3]. The change in enthalpy (ΔH_{bind}) was calculated as 32.6 kJ mol^{-1} based on an integration of the peak area (Table 2). The positive ΔH_{bind} value displayed energetically unfavorable endothermic binding reactions. The dissociation constant (K_d) obtained by fitting to the binding isotherm (see the Materials and Methods section) was 1.0 ± 0.1 μM (Table 2), which was similar to the value of K_m (Fig. S3A). The n value of approximately 0.8 suggested one-to-one binding stoichiometry between Fd and FNR. By using thermodynamic relationships, we obtained changes in free energy (ΔG_{bind}) and entropy ($-T\Delta S_{bind}$) (Table 2). Negative ΔG_{bind} (−34.2 ± 0.2 kJ mol^{-1}) and $-T\Delta S_{bind}$ (−66.8 ± 0.4 kJ mol^{-1}) indicated spontaneous Fd:FNR complex formation driven purely by positive ΔS_{bind}.

ITC measurements at 298 K were performed for S43W and S43D and endothermic binding heat was also detected (Fig. 3A). The

Table 1
Summary of various parameters of FNR enzymatic activity obtained by steady-state kinetics. The average and error values were obtained from measurements in triplicate.

Temperature (K)	Wild-type Fd		S43W Fd		S43D Fd	
	K_m (μM)	k_{cat} (s^{-1})	K_m (μM)	k_{cat} (s^{-1})	K_m (μM)	k_{cat} (s^{-1})
288	2.3 ± 0.3	37.8 ± 3.5	0.7 ± 0.0	37.8 ± 2.4	11.6 ± 1.2	35.9 ± 2.2
293	2.2 ± 0.2	44.7 ± 5.8	0.7 ± 0.0	43.9 ± 3.6	9.9 ± 0.8	40.5 ± 2.2
298	2.2 ± 0.3	53.5 ± 1.8	0.8 ± 0.0	56.8 ± 1.4	9.0 ± 0.4	50.7 ± 3.6
303	2.4 ± 0.3	72.5 ± 6.4	0.8 ± 0.1	66.9 ± 0.5	8.5 ± 0.5	65.5 ± 5.0
E_a (kJ mol^{-1})	31.1 ± 3.3		28.7 ± 3.7		29.3 ± 2.6	

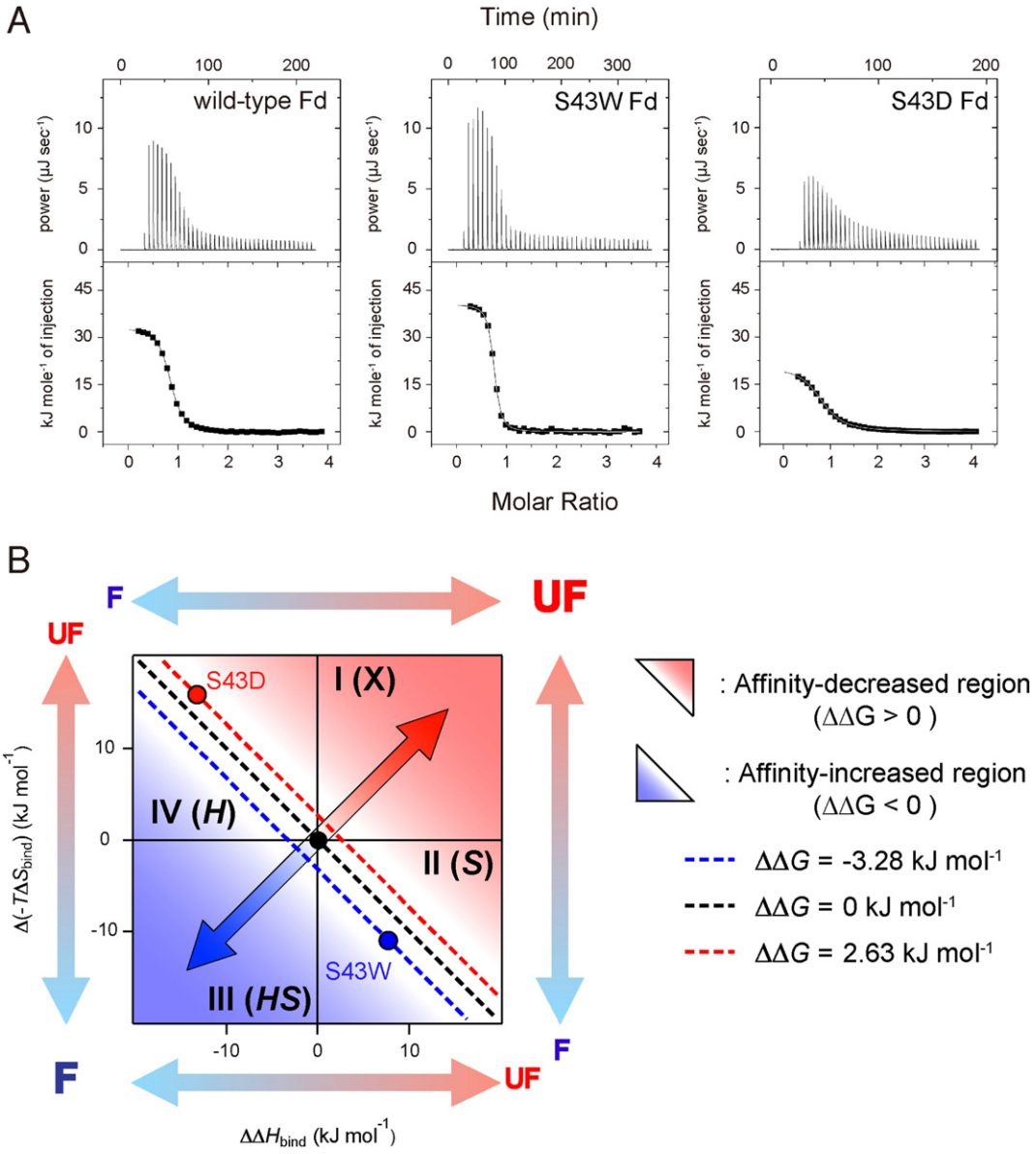

Fig. 3. Thermodynamic characterization of binding reactions between Fd and FNR using ITC and a driving force plot. (A) ITC thermograms of the titration of wild-type Fd (left), S43W Fd (middle), and S43D Fd (right) to FNR are shown in the upper panel. Normalized heat values were plotted against the molar ratio ([Fd]/[FNR]) in the lower panel. Fitted curves are exhibited using continuous lines. (B) Changes in the driving force (ΔH_{bind} and $-T\Delta S_{bind}$) and ΔG_{bind} value after the formation of each complex are shown. The broken diagonal lines in black, red, and blue signify the $\Delta\Delta G_{bind}$ lines of 0, 2.63, and −3.28 kJ mol^{-1}, respectively. Thermodynamically favorable and unfavorable directions on mutation are guided by blue arrows and "F" and red arrows and "UF", respectively, in and out of the panel. The blue and red triangular regions indicate increases and decreases in affinity. Transverse and longitudinal axes indicate $\Delta\Delta H_{bind}$ and $\Delta(-T\Delta S_{bind})$, respectively. The black sphere indicates no change in ΔG_{bind} (i.e., $\Delta\Delta G_{bind} = 0$). Red and blue spheres show $\Delta\Delta G_{bind}$ following changes in ΔG_{bind} with the mutation of serine at 43 to tryptophan (i.e., S43W) or aspartic acid (i.e., S43D), respectively. The four rectangular regions were classified by driving forces: region "I" (upper right), region "II" (lower right), region "III" (lower left), and region "IV" (upper left). In each region, a thermodynamically favorable driving force is indicated in parentheses. "I(X)" represents no driving force for favoring binding reactions.

thermodynamic and physical parameters analyzed (ΔH_{bind}, K_d, ΔG_{bind}, $-T\Delta S_{bind}$, and n) were summarized in Table 2. K_d values were similar to K_m: the K_d values of S43W (0.3 ± 0.1 μM) and S43D (3.0 ± 0.4 μM) were lower and higher than that of wild-type Fd (1.0 ± 0.1 μM), respectively (Fig. S3A). Therefore, the order of ΔG_{bind} was S43D (−31.6 ± 0.3 kJ mol^{-1}) > wild-type (−34.2 ± 0.2 kJ mol^{-1}) > S43W (−37.5 ± 0.7 kJ mol^{-1}) (Fig. S3B). The complex formation of FNR with Fd variants was also only favored by the positive entropy change (Fig. S3B). The ΔH_{bind} value was in the order of S43W (40.3 ± 0.5 kJ mol^{-1}) > wild-type (32.6 ± 0.2 kJ mol^{-1}) > S43D (19.4 ± 0.2 kJ mol^{-1}), and S43D (−51.0 ± 0.2 kJ mol^{-1}) > wild-type (−66.8 ± 0.4 kJ mol^{-1}) > S43W (−77.8 ± 0.3 kJ mol^{-1}) for the $-T\Delta S_{bind}$ value.

3.5. Temperature dependence of thermodynamic parameters for Fd:FNR complexation

The thermodynamic properties of interprotein interactions are a function of temperature. Thus, temperature-dependent changes in thermodynamic parameters reflect the influences of physicochemical properties on intermolecular interactions.

Therefore, we examined changes in various thermodynamic parameters for the interactions between wild-type Fd and FNR in the range of 288 to 303 K (Fig. 4). K_d values decreased from 1.5 ± 0.4 to 0.9 ± 0.2 μM with an increase in temperature from 288 to 303 K (Table 2). As observed for K_m values, K_d values also decreased from 1.5 ± 0.4 to 0.9 ± 0.2 μM with increases in temperature from 288

Table 2
Summary of various thermodynamics parameters of complex formation between Fd and FNR obtained by ITC. The average and error values were obtained from measurements in duplicate.

	Temperature (K)	K_d (μM)	ΔG_{bind} (kJ mol^{-1})	ΔH_{bind} (kJ mol^{-1})	$-T\Delta S_{bind}$ (kJ mol^{-1})	n
Wild-type Fd	288	1.5 ± 0.4	−32.1 ± 0.6	32.1 ± 0.5	−64.2 ± 0.1	0.8
	293	1.2 ± 0.1	−33.1 ± 0.2	32.6 ± 0.8	−65.8 ± 1.0	0.8
	298	1.0 ± 0.1	−34.2 ± 0.2	32.6 ± 0.2	−66.8 ± 0.4	0.8
	303	0.9 ± 0.2	−35.2 ± 0.5	30.7 ± 0.0	−65.9 ± 0.6	0.8
S43W Fd	288	0.6 ± 0.0	−34.5 ± 0.2	37.4 ± 2.6	−71.9 ± 2.8	0.7
	293	0.4 ± 0.0	−35.6 ± 0.1	38.7 ± 3.8	−74.3 ± 3.9	0.7
	298	0.3 ± 0.1	−37.5 ± 0.7	40.3 ± 0.5	−77.8 ± 0.3	0.7
	303	0.3 ± 0.0	−38.1 ± 0.2	35.5 ± 2.1	−73.6 ± 2.3	0.7
S43D Fd	288	4.7 ± 1.4	−29.5 ± 0.7	13.7 ± 0.0	−43.2 ± 0.7	0.9
	293	3.8 ± 1.0	−30.5 ± 0.7	16.5 ± 1.2	−47.1 ± 0.6	0.8
	298	3.0 ± 0.4	−31.6 ± 0.3	19.4 ± 0.2	−51.0 ± 0.2	0.8
	303	2.4 ± 0.9	−32.8 ± 1.0	21.2 ± 2.0	−54.0 ± 1.0	0.8

to 303 K (Table 2), indicating an increase in interprotein affinity with a decrease in ΔG_{bind} by −3.1 kJ mol^{-1} (Fig. 4A). ΔH_{bind} and $-T\Delta S_{bind}$ both became gradually favorable with increases in temperature from 32.1 ± 0.6 kJ mol^{-1} at 288 K to 30.7 ± 0.0 kJ mol^{-1} at 303 K and from −64.2 ± 0.1 kJ mol^{-1} at 288 K to −65.9 ± 0.6 kJ mol^{-1} at 303 K, respectively. These results revealed that the two energetic terms were stabilizers for the Fd:FNR complex regardless of the temperatures examined here.

The binding of S43W to FNR showed similar temperature responses to those of wild-type Fd. However, the temperature dependence of ΔH_{bind} and $-T\Delta S_{bind}$ for S43D binding was markedly different. ΔH_{bind} values markedly increased from 13.7 ± 0.0 kJ mol^{-1} at 288 K to 21.2 ± 2.0 kJ mol^{-1} at 303 K (Fig. 4C), whereas and $-T\Delta S_{bind}$ values markedly decreased from −43.2 ± 0.7 kJ mol^{-1} at 288 K to −54.0 ± 1.0 kJ mol^{-1} at 303 K (Fig. 4B).

The change in heat capacity (ΔC_p) was obtained from the slope of the temperature dependence of ΔH_{bind} (i.e., $\partial\Delta H_{bind}/\partial T$). Although the ΔC_p values of wild-type and S43W binding to FNR were similar to each other, that of S43D binding was largely distinct. The ΔC_p values for the binding of wild-type Fd, S43W, and S43D to FNR were −87, −76, and 507 J mol^{-1} K^{-1}, respectively (Fig. 4D and Table 2).

No clear decrease was observed in K_m for wild-type and S43W Fds with increases in temperature (Table 1); however, increases in temperature led to reductions in K_d for all three types of Fds (Table 2). Although

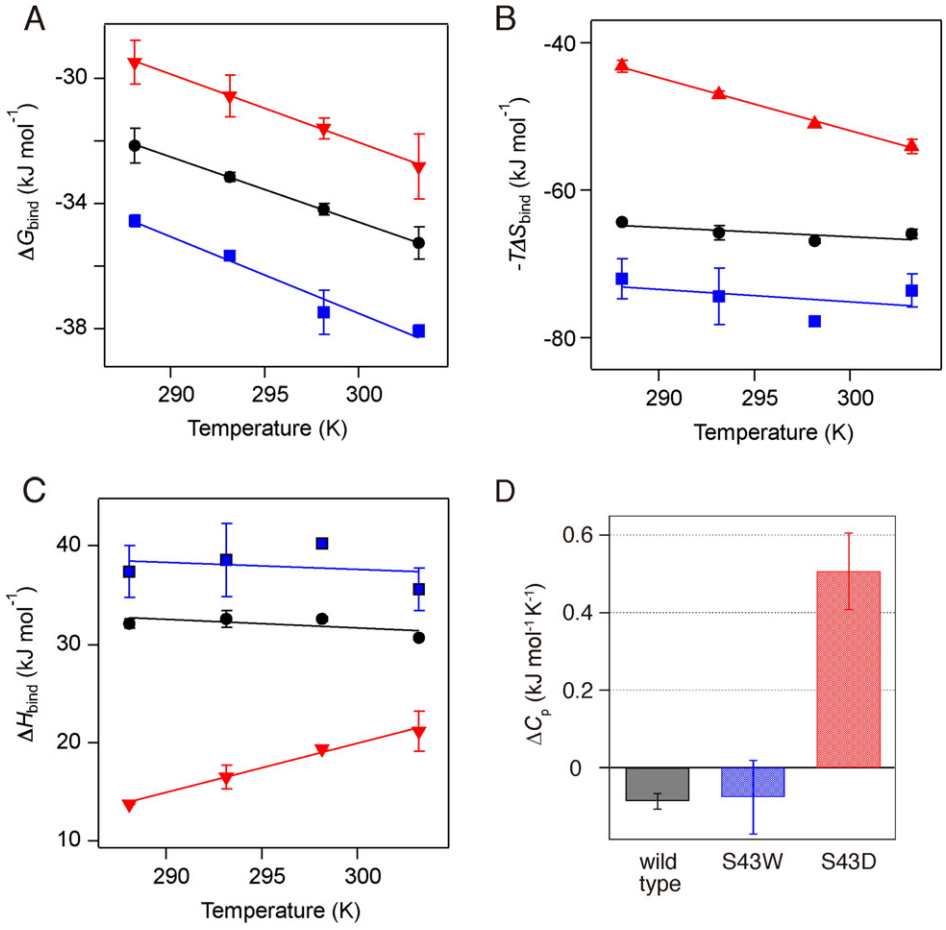

Fig. 4. Temperature-dependent thermodynamic parameters. (A–C) The values of ΔG_{bind} (A), $-T\Delta S_{bind}$ (B), and ΔH_{bind} (C) were plotted as a function of temperature. (D) The ΔC_p values of wild-type, S43W, and S43D Fds are shown. Thermodynamic parameters for FNR binding to wild-type, S43W, and S43D Fds are shown in black, blue, and red, respectively.

the underlying mechanism and reason for these discrepancies remain unclear, the physical binding properties of K_d between complexes and free proteins directly obtained by the thermodynamic measurement of ITC may not be always consistent with K_m obtained from Michaelis–Menten kinetics depending on changes in temperature. The components present in reconstituted activity assay systems, but absent in ITC measurement systems, such as cytochrome *c*, may be involved in distinct responses between K_d and K_m at different temperatures. Alternatively, the distinct approaches utilized produced different values to some extent, which is often observed in K_d values obtained by different methods such as ITC, NMR, and surface plasmon resonance [36,37].

3.6. Residue-based investigation of Fd–FNR interactions using NMR spectroscopy

In order to obtain more detailed information on the binding mode and interfaces of FNR for Fds at the residue level, two-dimensional ^{1}H–^{15}N HSQC measurements on uniformly-labeled FNR with ^{15}N were performed in the absence and presence of Fds (wild-type, S43W, and S43D) (Fig. 5A).

The NMR cross-peaks of FNR in the absence of Fd were sharp and widely dispersed, which indicated the well-folded state of FNR. Based on the K_d values obtained from ITC measurements, the amounts of Fd added were 2-fold that of FNR in order to saturate FNR with Fd. The

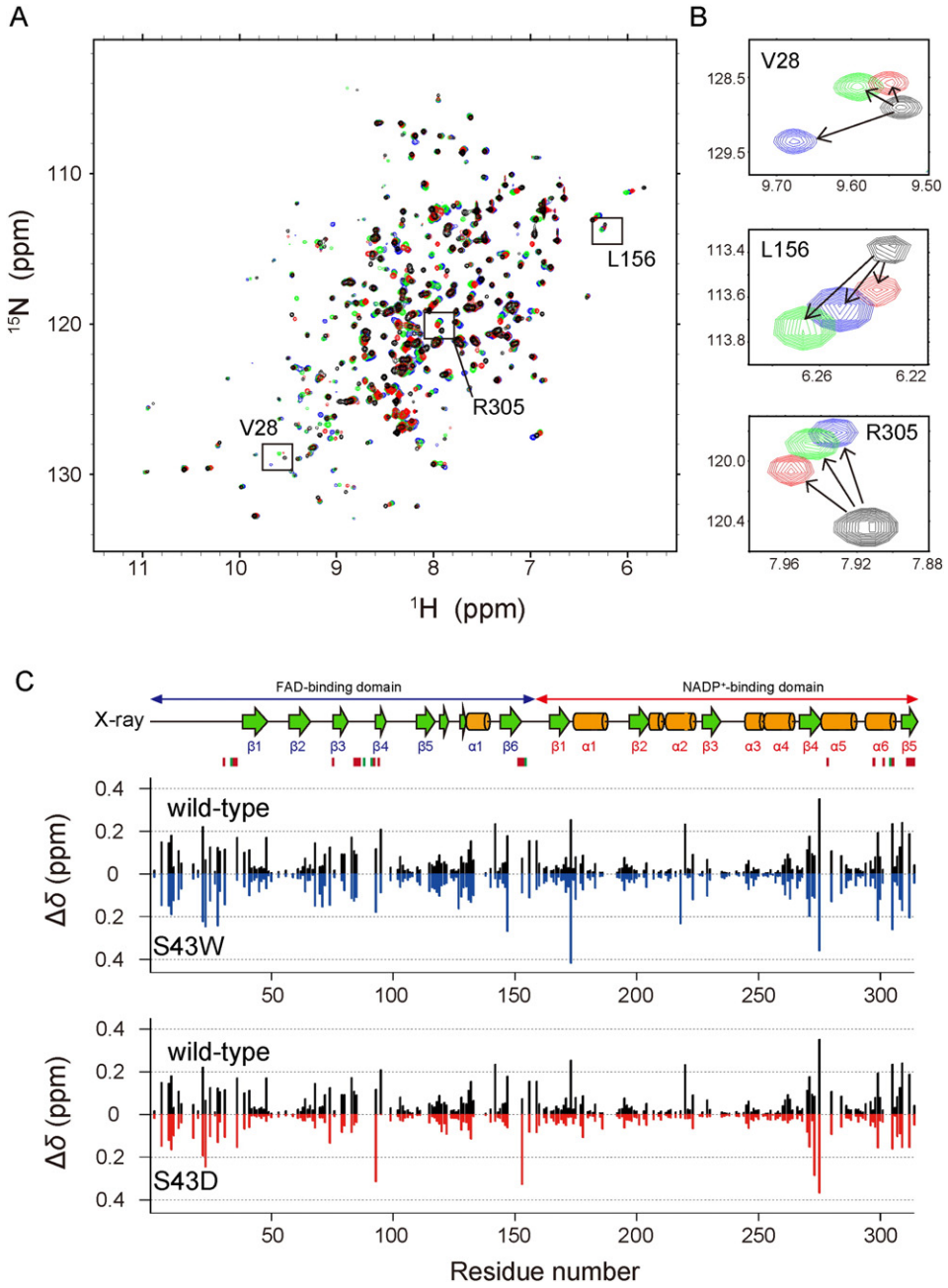

Fig. 5. NMR spectroscopy of ^{15}N-labeled FNR with and without Fd and chemical shift perturbation analyses. (A) The superposition of ^{1}H–^{15}N HSQC spectra of FNR without Fd (black) and with wild-type (green), S43W (blue), or S43D Fds (red). (B) Shifts in the peak (V28, L156, and R305) are representatively magnified. (C) Chemical shift perturbations with the addition of each type of Fd were plotted against the residue number of FNR. The secondary structure elements determined from the X-ray structure (PDB/1GAW) are displayed in the top part. Alpha-helices and beta-strands are colored in orange and green, respectively. The residues of FNR interacting with Fd are shown by the colored rectangles below the secondary structure elements. Green and red indicate positively-charged and non-charged residues, respectively.

population of each Fd:FNR complex was close to 100%. The addition of each Fd changed a large number of the NMR peak positions of FNR without significantly altering the number of peaks in the absence of Fds (Fig. 5A). This result indicated the formation of individual Fd:FNR complexes and a fast exchange regime of interactions between each Fd and FNR.

Although the direction of changes in peak shifts depended on the types of Fd (Fig. 5B), the overall perturbed regions of FNR were all similar, as shown by the plot of the chemical shift perturbation (CSP) (Fig. 5C) and mapping of CSP values on a crystal structure of FNR (Fig. S4). These results were consistent with our previous findings [18]. Perturbed residues were mainly located in the N-terminal and β2–β3 (around K88 and K91) regions on the FAD-binding domain, the interdomain region around D154, and the β1–α1 (around G173), β4–α5 (around K275), and C-terminal (around K304) regions on the $NADP^+$-binding domain, which is in accordance with those suggested by the crystal structure of the wild-type Fd:FNR complex [22]. The hydrophobic residues of I68, V83, I147, and L156 and polar residues of T29, Q74, and C132 also showed perturbations.

The representative residues that showed large perturbations regardless of the types of Fd were in the N- and C-terminal regions and also in the β4–α5 region around K275. R93 and K153 of FNR in the presence of S43D showed larger CSP values than those in the presence of wild-type Fd.

4. Discussion

4.1. Importance of hydrophobic and electrostatic residues of Fd for activities of partner enzymes

The electrostatic interaction between Fd and a partner enzyme has predominantly been reasoned as a key contributor to the efficient activity of a partner enzyme. However, we questioned this interpretation because the buried nonpolar surface area of the Fd:FNR complex was previously shown to account for approximately 50% of the total buried apolar surface area [22]. Therefore, we focused on the effects of the physicochemical properties of interfacial residues around the [2Fe–2S] cluster from the viewpoint of enzyme activity by addressing hydrophobic and electrostatic contributions.

Partner enzyme-dependent activity changes in most of the tryptophan mutants, except for S45W (Fig. 1C and D), demonstrated that hydrophobic interactions on binding interfaces around S38 to S46 of Fd, which have not received much attention, were essential for the regulation of FNR and SiR activities. A set of S43 mutants also showed the contribution of hydrophobic forces to changes in activity depending on partner enzymes. A similar finding was also reported in the plant-type photosynthetic electron transport ferredoxin (PETF) [17]. The PETF mutants, D19A and D58A, exhibited the differential recognition and activity between FNR and hydrogenase HYDA1.

Partner enzyme-dependent activity changes in S43 mutants (S43H and S43D) provided further insights into electrostatic contributions (Fig. 1E and F). S43H, which increased the repulsive charge–charge interaction with Fd, decreased SiR activity, but had no effects on FNR activity. In contrast to the general expectation that attractive electrostatic interactions increase activity, S43D exhibited a decrease in FNR activity without a change in SiR activity.

Taken together, our results suggested that activity changes were not always predictable by the general electrostatic contribution alone, and the physicochemical properties of hydrophobic and electrostatic residues on interprotein interfaces were important in the regulation of FNR and SiR activities.

4.2. Interprotein interactions dominated FNR activity

The overall activity of FNR comprised physical processes including intermolecular interactions among Fd, FNR, and the substrate of $NADP^+$ as well as the chemical reactions of electron and hydride transfer.

In order to identify the dominant factor regulating FNR activity, we introduced a site-directed mutation to Fd because a mutation in FNR may include changes in the intrinsic catalytic capability of FNR as well as in the intermolecular interaction with Fd and $NADP^+$. By mutating Fd, we expected a simpler system that predominantly reflected a mutation effect stemming from interprotein interactions directly linked to interprotein electron flow from FNR to Fd.

We again selected the two mutants of Fd that displayed the most prominent changes in enzymatic activity (Fig. 1E and F), S43W and S43D. Although no appreciable alternations were observed in the chemical reaction (k_{cat}) or activation energy (E_a) for S43W and S43D (Fig. 2B and C), physical changes identified in K_m indicated that the interprotein interaction was a dominant factor controlling the overall activity of FNR (Fig. 2). The similar dependence of changes in enzymatic activities due to interprotein interactions was observed in other electron transfer proteins. We previously reported that changes in enzymatic activities by the neutralization of acidic residues on the binding surfaces of Fd for SiR [24] and NiR [9] primarily depended on K_m values, not k_{cat} values. Similar findings were also found in cytochrome *c*-related electron transfer and activity assays [38].

Our results and previous findings demonstrated that physicochemical properties at the location of 43 on the interface of Fd were important for determining overall FNR activity by adjusting interprotein interactions between Fd and FNR. Furthermore, we suggested that this concept may be applicable to other enzyme activity studies utilizing electron-transport proteins.

4.3. Fd–FNR interactions under thermodynamic controls

Since physical interactions between Fd and FNR regulated FNR activity and interprotein interactions were fundamentally under thermodynamic control, binding energetics between two proteins were characterized at the molecular level using ITC (Figs. 3 and 4). ITC is one of the most powerful approaches for elucidating the physical, mechanical, and energetic natures of binding systems including molecular association mechanisms, binding modes, and driving forces for complexation [2,3,39].

Complexation-interrupting positive ΔH_{bind} values were detected in all complexes formed as a result of energy costs for the dehydration of charged residues, which drove complex formation solely with entropy (Fig. S3B) [3]. The higher affinity of S43W for FNR than the wild-type was attributed to the gain of entropy (increases in ΔS_{bind}), which overwhelmed the unfavorable enthalpic loss (increases in ΔH_{bind}) (Fig. S3B), as shown in the driving force plot (Fig. 3B). The dehydration of water from hydrophobic regions around the tryptophan residue, i.e., the hydrophobic effect, and electrostatic/polar regions may have largely stabilized the Fd:FNR complex.

The driving force plot rationalized the weakened affinity of S43D for FNR with the loss of $\Delta\Delta G = 2.63$ kJ mol^{-1} in terms of the penalty of entropy (Figs. 3B and S3B). The formation of an electrostatic and hydrogen bond network around the negative charge of the aspartic acid at 43 (Fig. 3B) may have engendered favorable contributions to the formation of the S43D:FNR complex by reducing ΔH_{bind}. Furthermore, since attractive intermolecular interactions have been shown to promote molecular recognition [40], a decrease in affinity may also be kinetically explained by a markedly faster dissociation rate than association rate.

Electrostatic and hydrophobic interactions are a function of temperature. Elevations in temperature are generally accepted to be accompanied by reductions in electrostatic forces and the reinforcement of hydrophobic forces [41,42]. Hence, perturbations to a binding system by changes in temperature support an informative measure of the relative contributions of these two intermolecular forces to complex formation. In all three binding systems, ΔG_{bind} decreased linearly with increases in temperature (Fig. 4A). Furthermore, ΔC_p, a thermodynamic

indicator of physicochemical properties for the buried surface area, showed small negative values for wild-type Fd:FNR binding and S43W:FNR binding, which demonstrated that the thermodynamic contributions of buried hydrophobic surface areas were slightly more dominant than those of electrostatic/polar surface areas. These results indicated the thermodynamic importance of hydrophobic forces in stabilizing the Fd:FNR complex (Fig. 4D). A positive ΔC_p value was obtained for S43D:FNR binding, which was suggestive of the large contribution of the burial of electrostatic/polar surface areas. A positive ΔC_p was previously observed in binding reactions between nucleic acids and proteins or in protein misfolding and aggregation due to the burial of charges [43].

Distinct individual thermodynamic parameters for complexation depending on the type of Fds proposed different binding modes and/or orientations of individual Fds to FNR, which were fit toward maximizing energetic merits for physical interactions between proteins under given conditions. Our comprehensive driving force plot showed the capability of proteins for thermodynamic trades based on enthalpy–entropy compensation, which may be one of the properties of evolution pressure (Fig. 3B).

4.4. Interfacial physicochemical properties determined the physical binding mode between Fd and FNR

A residue-based investigation with NMR spectroscopy provided further insights into interprotein interactions. Although the plotting and mapping of CSP indicated the similar binding interfaces of FNR for each Fd (Figs. 5C and S4), the direction of shifts in many peaks such as V28, L156, and R305 differed depending on the type of Fd (Fig. 5B). This was mostly attributed to the distinct strength of hydrogen bonds, backbone dihedral angles, and influences of surrounding residues [44], which reflected an alternative binding mode and/or orientation between proteins.

The visualization of the three Fd:FNR complexes by a docking simulation with the incorporation of the CSP of NMR as a restraint (Fig. 6A) revealed detailed images of binding interfaces (Fig. 6B–E). Binding

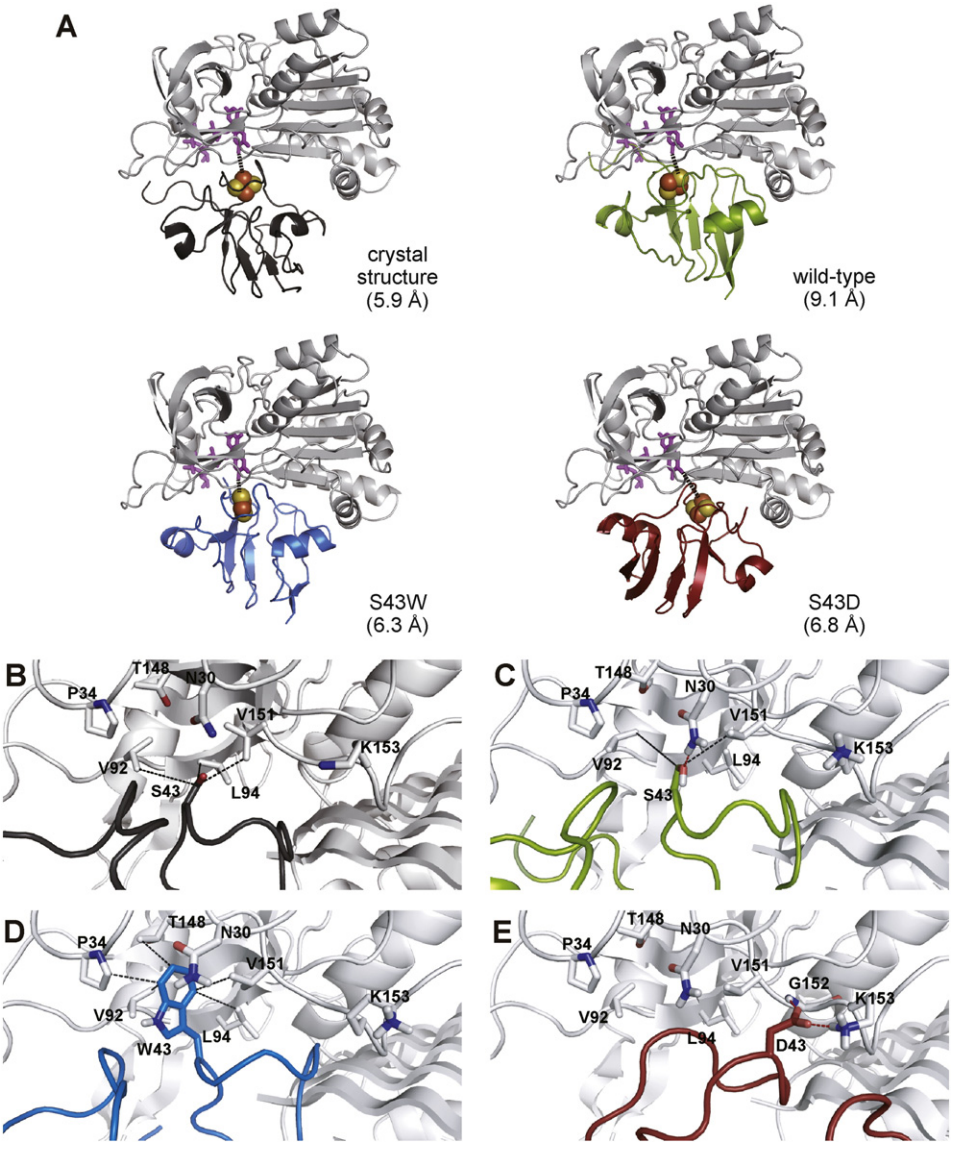

Fig. 6. Modeled Fd:FNR complexes and their binding interfaces. (A) The complex structures of wild-type Fd and FNR determined by X-ray crystallography and three docking simulation structures with HADDOCK in combination with NMR data are shown. Each complex, which showed the lowest energy, was selected from 40 complexes. FNR is colored in gray. Wild-type, S43W, and S43D Fds are shown in green, blue, and red, respectively. Magenta sticks in FNR indicate FAD. Red and yellow spheres in Fd represent iron and sulfur, respectively. The distance between FAD and iron guided by the broken line is shown in parentheses. (B, C) Interprotein surfaces between FNR and wild-type Fd determined by X-ray crystallography (B) and a docking simulation with HADDOCK in combination with NMR data (C) are magnified for comparisons. (D, E) The interacting surfaces between FNR and S43W Fd (D) or S43D Fd (E), as modeled by HADDOCK, are also shown.

interfaces between wild-type Fd and FNR consisted of electrostatic and hydrophobic interactions together with polar interactions including several H-bonds (Fig. 6C). Serine at 43 of Fd formed several hydrogen bonds with the neighboring residues of V92, L94, and V151 of FNR. Although interactions between interfacial residues were similar in solutions (Fig. 6C) and crystals (Fig. 6B), the binding interfaces in solutions were wider to some extent than those in crystals (Figs. 5C and 6A–C), which implicated the more flexible binding of Fd and FNR in solution in favor of matching and tuning courses for a preferable complex conformation.

The binding interface of the S43W:FNR complex showed the insertion of the indole side chain of tryptophan at 43 of Fd to a small binding cavity of FNR through various non-covalent interactions with the side chains of FNR; however, the orientation of Fd differed from that of wild-type Fd (Fig. 6D).

Although interacting sites between the surface of S43D around an aspartic acid at 43 and FNR led to predominant electrostatic interactions (Fig. 6E), the interacting site of FNR for Fd shifted to a more central part of FNR, a loop between the FAD- and $NADP^+$-binding domains, than wild-type Fd and S43W binding. The negative charge of aspartic acid at 43 formed a salt bridge with the positive charge of a lysine residue (K153) and a hydrogen bond with the backbone of a glycine (G152). These intermolecular electrostatic networks provide a clue for the positive value of ΔC_p due to the burial of charges (Fig. 4D).

The orientation between Fd and FNR was appropriate for interprotein electron transfer. The distance between the isoalloxazine ring in FAD and iron in the [2Fe–2S] cluster in each Fd:FNR complex was sufficiently small in all cases (6.3 Å–9.1 Å) (Fig. 6A–D) for electron transfer to not be rate-limiting. These results suggested that the binding mode and orientation of each Fd to FNR were different at the residue level and this physical interprotein binding was changeable through alternations in the physicochemical properties of the interfacial residues of Fd by means of varying electrostatic and hydrophobic natures.

4.5. Thermodynamic and physical balances of non-covalent intermolecular interactions limited FNR activity

We previously demonstrated that the entropic gain from conformational flexibility and dehydration was the only driving force for the complex formation of Fd and FNR under mildly acidic conditions in spite of the formation of five salt bridges [3]. We herein obtained a more detailed rationale by combining biochemical and biophysical approaches as well as an improved understanding of the molecular origins of the regulation of FNR activity.

Large increases in favorable electrostatic interactions may be disadvantageous for the best orientation for intermolecular electron transfer and/or weakened interprotein affinity, thereby decreasing activity, as observed in the binding of S43D with FNR (Figs. 3B and 6E). On the one hand, large increases in hydrophobicity may promote faster sampling of the conformational space of complex structures by taking advantage of short-range hydrophobic interactions and, in turn, reaching a more optimal complex structure with high stability, thereby enhancing FNR activity by increasing the rate of electron transfer and interprotein affinity (Figs. 2, 3B, and 6D).

Therefore, even a single mutation in a hydrophobic environment without the disruption of Fd integrity is sufficient to limit overall FNR activity through the delicate balance of enthalpy and entropy in the form of non-covalent interactions and dehydration, which determines interprotein affinity and orientation (Fig. 3B). Further systematic studies using SiR and/or SiR and FNR mutants are required to obtain more general conclusions.

We suggest that proteins sensitively cope with changes in environmental conditions and spontaneous mutations in a thermodynamically favorable way to reduce global energy. However, an enzyme responds in a functionally favorable way, including thermodynamics and kinetics.

Transparency Document

The Transparency Document associated with this article can be found, in online version.

Acknowledgments

We thank Prof. Yuji Goto (Osaka University, Japan) for his valuable comments. This work was supported by a Grant-in-Aid for Young Scientists (B) (15K18518 and 25870407) for Y.-H. Lee and Platform for Drug Discovery, Informatics, and Structural Life Science from the Ministry of Education, Culture, Sports, Science and Technology, Japan.

Appendix A. Supplementary data

Supplementary data to this article can be found online at http://dx.doi.org/10.1016/j.bbabio.2015.05.023.

References

[1] R. Gilli, D. Lafitte, C. Lopez, M. Kilhoffer, A. Makarov, C. Briand, J. Haiech, Thermodynamic analysis of calcium and magnesium binding to calmodulin, Biochemistry 37 (1998) 5450–5456.
[2] S. Kume, Y.H. Lee, M. Nakatsuji, Y. Teraoka, K. Yamaguchi, Y. Goto, T. Inui, Fine-tuned broad binding capability of human lipocalin-type prostaglandin D synthase for various small lipophilic ligands, FEBS Lett. 588 (2014) 962–969.
[3] Y.H. Lee, T. Ikegami, D.M. Standley, K. Sakurai, T. Hase, Y. Goto, Binding energetics of ferredoxin-$NADP^+$ reductase with ferredoxin and its relation to function, Chembiochem 12 (2011) 2062–2070.
[4] D. Eisenberg, M. Jucker, The amyloid state of proteins in human diseases, Cell 148 (2012) 1188–1203.
[5] G. Hanke, P. Mulo, Plant type ferredoxins and ferredoxin-dependent metabolism, Plant Cell Environ. 36 (2013) 1071–1084.
[6] C.J. Batie, H. Kamin, Electron transfer by ferredoxin:$NADP^+$ reductase. Rapid-reaction evidence for participation of a ternary complex, J. Biol. Chem. 259 (1984) 11976–11985.
[7] D.G. Bishop, K.S. Andersen, R.M. Smillie, pH Dependence and cofactor requirements of photochemical reactions in maize chloroplasts, Plant Physiol. 50 (1972) 774–777.
[8] A. Sanchez-Azqueta, M. Martinez-Julvez, M. Hervas, J.A. Navarro, M. Medina, External loops at the ferredoxin-$NADP(^+)$ reductase protein-partner binding cavity contribute to substrates allocation, Biochim. Biophys. Acta 1837 (2014) 296–305.
[9] Y. Sakakibara, H. Kimura, A. Iwamura, T. Saitoh, T. Ikegami, G. Kurisu, T. Hase, A new structural insight into differential interaction of cyanobacterial and plant ferredoxins with nitrite reductase as revealed by NMR and X-ray crystallographic studies, J. Biochem. 151 (2012) 483–492.
[10] P. Mulo, Chloroplast-targeted ferredoxin-$NADP(^+)$ oxidoreductase (FNR): structure, function and location, Biochim. Biophys. Acta 1807 (2011) 927–934.
[11] T. Saitoh, T. Ikegami, M. Nakayama, K. Teshima, H. Akutsu, T. Hase, NMR study of the electron transfer complex of plant ferredoxin and sulfite reductase: mapping the interaction sites of ferredoxin, J. Biol. Chem. 281 (2006) 10482–10488.
[12] A. Sali, Comparative protein modeling by satisfaction of spatial restraints, Mol. Med. Today 1 (1995) 270–277.
[13] S.R. Tzeng, C.G. Kalodimos, Protein activity regulation by conformational entropy, Nature 488 (2012) 236–240.
[14] R.V. Duran, M. Hervas, M.A. De La Rosa, J.A. Navarro, The efficient functioning of photosynthesis and respiration in *Synechocystis* sp. PCC 6803 strictly requires the presence of either cytochrome c_6 or plastocyanin, J. Biol. Chem. 279 (2004) 7229–7233.
[15] M. Hippler, J. Reichert, M. Sutter, E. Zak, L. Altschmied, U. Schroer, R.G. Herrmann, W. Haehnel, The plastocyanin binding domain of photosystem I, EMBO J. 15 (1996) 6374–6384.
[16] J.B. Asbury, E. Hao, Y. Wang, H.N. Ghosh, T. Lian, Ultrafast electron transfer dynamics from molecular adsorbates to semiconductor nanocrystalline thin films, J. Phys. Chem. B 105 (2001) 4545–4557.
[17] S. Rumpel, J.F. Siebel, C. Fares, J. Duan, E. Reijerse, T. Happe, W. Lubitz, M. Winkler, Enhancing hydrogen production of microalgae by redirecting electrons from photosystem I to hydrogenase, Energy Environ. Sci. 7 (2014) 3296–3301.
[18] M. Maeda, Y.H. Lee, T. Ikegami, K. Tamura, M. Hoshino, T. Yamazaki, M. Nakayama, T. Hase, Y. Goto, Identification of the N- and C-terminal substrate binding segments of ferredoxin-$NADP^+$ reductase by NMR, Biochemistry 44 (2005) 10644–10653.
[19] Y. Onda, T. Matsumura, Y. Kimata-Ariga, H. Sakakibara, T. Sugiyama, T. Hase, Differential interaction of maize root ferredoxin:$NADP(^+)$ oxidoreductase with photosynthetic and non-photosynthetic ferredoxin isoproteins, Plant Physiol. 123 (2000) 1037–1045.
[20] G.T. Hanke, Y. Satomi, K. Shinmura, T. Takao, T. Hase, A screen for potential ferredoxin electron transfer partners uncovers new, redox dependent interactions, Biochim. Biophys. Acta 1814 (2011) 366–374.
[21] D.B. Knaff, M. Hirasawa, Ferredoxin-dependent chloroplast enzymes, Biochim. Biophys. Acta 1056 (1991) 93–125.

[22] G. Kurisu, M. Kusunoki, E. Katoh, T. Yamazaki, K. Teshima, Y. Onda, Y. Kimata-Ariga, T. Hase, Structure of the electron transfer complex between ferredoxin and ferredoxin-NADP(+) reductase, Nat. Struct. Mol. Biol. 8 (2001) 117–121.
[23] P.A. Karplus, M.J. Daniels, J.R. Herriott, Atomic structure of ferredoxin-NADP+ reductase: prototype for a structurally novel flavoenzyme family, Science 251 (1991) 60–66.
[24] M. Nakayama, T. Akashi, T. Hase, Plant sulfite reductase: molecular structure, catalytic function and interaction with ferredoxin, J. Inorg. Biochem. 82 (2000) 27–32.
[25] M. Martinez-Julvez, M. Medina, A. Velazquez-Campoy, Binding thermodynamics of ferredoxin:NADP+ reductase: two different protein substrates and one energetics, Biophys. J. 96 (2009) 4966–4975.
[26] A. Aliverti, M.E. Corrado, G. Zanetti, Involvement of lysine-88 of spinach ferredoxin-NADP+ reductase in the interaction with ferredoxin, FEBS Lett. 343 (1994) 247–250.
[27] F.J. Enguita, E. Pohl, D.L. Turner, H. Santos, M.A. Carrondo, Structural evidence for a proton transfer pathway coupled with haem reduction of cytochrome c from *Methylophilus methylotrophus*, J. Biol. Inorg. Chem. 11 (2006) 189–196.
[28] T. Hase, S. Mizutani, Y. Mukohata, Expression of maize ferredoxin cDNA in *Escherichia coli*: comparison of photosynthetic and nonphotosynthetic ferredoxin isoproteins and their chimeric molecule, Plant Physiol. 97 (1991) 1395–1401.
[29] T. Matsumura, Y. Kimata-Ariga, H. Sakakibara, T. Sugiyama, H. Murata, T. Takao, Y. Shimonishi, T. Hase, Complementary DNA cloning and characterization of ferredoxin localized in bundle-sheath cells of maize leaves, Plant Physiol. 119 (1999) 481–488.
[30] Y.H. Lee, K. Tamura, M. Maeda, M. Hoshino, K. Sakurai, S. Takahashi, T. Ikegami, T. Hase, Y. Goto, Cores and pH-dependent dynamics of ferredoxin-NADP+ reductase revealed by hydrogen/deuterium exchange, J. Biol. Chem. 282 (2007) 5959–5967.
[31] W. Lee, M. Tonelli, J.L. Markley, NMRFAM-SPARKY: enhanced software for biomolecular NMR spectroscopy, Bioinformatics 31 (2014) 1325–1327.
[32] R. Luthy, J.U. Bowie, D. Eisenberg, Assessment of protein models with three-dimensional profiles, Nature 356 (1992) 83–85.
[33] C. Dominguez, R. Boelens, A.M. Bonvin, HADDOCK: a protein–protein docking approach based on biochemical or biophysical information, J. Am. Chem. Soc. 125 (2003) 1731–1737.
[34] L. Willard, A. Ranjan, H. Zhang, H. Monzavi, R.F. Boyko, B.D. Sykes, D.S. Wishart, VADAR: a web server for quantitative evaluation of protein structure quality, Nucleic Acids Res. 31 (2003) 3316–3319.
[35] J.K. Hurley, A.M. Weber-Main, M.T. Stankovich, M.M. Benning, J.B. Thoden, J.L. Vanhooke, H.M. Holden, Y.K. Chae, B. Xia, H. Cheng, J.L. Markley, M. Martinez-Julvez, C. Gomez-Moreno, J.L. Schmeits, G. Tollin, Structure–function relationships in Anabaena ferredoxin: correlations between X-ray crystal structures, reduction potentials, and rate constants of electron transfer to ferredoxin:NADP+ reductase for site-specific ferredoxin mutants, Biochemistry 36 (1997) 11100–11117.
[36] S. Chhabra, O. Dolezal, B.M. Collins, J. Newman, J.S. Simpson, I.G. Macreadie, R. Fernley, T.S. Peat, J.D. Swarbrick, Structure of *S. aureus* HPPK and the discovery of a new substrate site inhibitor, PLoS ONE 7 (2012) e29444.
[37] E. Meiby, H. Simmonite, L. le Strat, B. Davis, N. Matassova, J.D. Moore, M. Mrosek, J. Murray, R.E. Hubbard, S. Ohlson, Fragment screening by weak affinity chromatography: comparison with established techniques for screening against HSP90, Anal. Chem. 85 (2013) 6756–6766.
[38] Y. Zhen, C.W. Hoganson, G.T. Babcock, S. Ferguson-Miller, Definition of the interaction domain for cytochrome c on cytochrome c oxidase. I. Biochemical, spectral, and kinetic characterization of surface mutants in subunit ii of Rhodobacter sphaeroides cytochrome aa_3, J. Biol. Chem. 274 (1999) 38032–38041.
[39] V. Ball, C. Maechling, Isothermal microcalorimetry to investigate non specific interactions in biophysical chemistry, Int. J. Mol. Sci. 10 (2009) 3283–3315.
[40] H.X. Zhou, Disparate ionic-strength dependencies of on and off rates in protein–protein association, Biopolymers 59 (2001) 427–433.
[41] K. Koga, Osmotic second virial coefficient of methane in water, J. Phys. Chem. B 117 (2013) 12619–12624.
[42] S. Kumar, R. Nussinov, Different roles of electrostatics in heat and in cold: adaptation by citrate synthase, Chembiochem 5 (2004) 280–290.
[43] T. Ikenoue, Y.H. Lee, J. Kardos, H. Yagi, T. Ikegami, H. Naiki, Y. Goto, Heat of supersaturation-limited amyloid burst directly monitored by isothermal titration calorimetry, Proc. Natl. Acad. Sci. 111 (2014) 6654–6659.
[44] S. Neal, A.M. Nip, H. Zhang, D.S. Wishart, Rapid and accurate calculation of protein ^{1}H, ^{13}C and ^{15}N chemical shifts, J. Biomol. NMR 26 (2003) 215–240.